Working-fluid replacement in supersonic organic Rankine cycle turbines

Martin T. White
Research Associate
Department of Mechanical Engineering and Aeronautics,
City, University of London,
Northampton Square,
London, EC1V 0HB
Email: martin.white@city.ac.uk

Christos N. Markides
Head of the Clean Energy Processes (CEP) Laboratory,
Department of Chemical Engineering,
Imperial College London,
South Kensington Campus,
London, SW7 2AZ
Email: c.markides@imperial.ac.uk

Abdulnaser I. Sayma*
Professor of Energy Engineering
Department of Mechanical Engineering and Aeronautics,
City, University of London,
Northampton Square,
London, EC1V 0HB
Email: a.sayma@city.ac.uk

In this paper the effect of working-fluid replacement within an organic Rankine cycle turbine is investigated by evaluating the performance of two supersonic stators operating with different working fluids. After designing the two stators, intended for operation with R245fa and Toluene with stator exit absolute Mach numbers of 1.4 and 1.7 respectively, the performance of each stator is evaluated using ANSYS CFX. Based on the principle that the design of a given stator is dependent on the amount of flow turning, it is hypothesised that a stator's design point can be scaled to alternative working fluids by conserving the Prandtl-Meyer function and the polytropic index within the nozzle. A scaling method is developed and further CFD simulations for the scaled operating points verify that the Mach number distributions within the stator, and the non-dimensional velocity triangles at the stator exit, remain unchanged. This confirms that the method developed can predict stator performance following a change in the working fluid. Finally, a study investigating the effect of working-fluid replacement on the thermodynamic cycle is completed. The results show that the same turbine could be used in different systems with power outputs varying between 17 and 112 kW, suggesting the potential of matching the same turbine to multiple heat sources by tailoring the working fluid selected. This further implies that the same turbine design could be deployed in different applications, thus leading to economy-of-scale improvements.

Nomenclature

a	speed of sound, m/s
b	blade height, m
c	velocity, m/s
D	turbine rotor diameter, m
h	enthalpy, J/kg
J	non-classical flow parameter
k	polytropic index
$\dot{m}$	mass-flow rate, kg/s
Ma	Mach number
N	rotational speed, rpm
N_s	specific speed
o_{th}	throat size, m
P	pressure, kPa
r	radius, m
R	specific gas constant, J/kg
Re	Reynolds number
s	entropy, J/(kg K)
T	temperature, K
u	blade velocity, m/s
$\dot{W}$	power, J/s
z	compressibility factor
Z_n	number of stator vanes
α	absolute flow angle, $^\circ$
β	relative flow angle, $^\circ$
Γ	fundamental derivative
ζ_n	stator loss coefficient
η	isentropic efficiency, %

*Corresponding author: a.sayma@city.ac.uk

μ	viscosity, Pa s
ν	Prandtl-Meyer function, $^\circ$
ν_{ts}	isentropic velocity ratio
ξ	loss coefficient
ρ	density, kg/m^3
ϕ	flow coefficient
ψ	blade-loading coefficient

Subscripts

0	total conditions
1	turbine inlet
4	rotor inlet
5	rotor outlet
c	condensation
cr	critical point
d	design point
le	leading edge
s	isentropic process
t	turbine
te	trailing edge
ts	total to static
*	choked throat

1 Introduction

Organic Rankine cycle (ORC) systems with power outputs exceeding a few hundred kilowatts are a mature technology for the conversion of low- and medium-temperature heat sources into shaft power [1, 2]. By comparison, there is a significant interest in smaller ORC systems for domestic and commercial-scale combined heat and power [3] and solar [4, 5] applications, alongside engine waste-heat recovery [6]. However, the widespread implementation of these technologies is currently limited by a lack of suitable expanders, and high system costs. The development of an efficient expander that can be manufactured at a low cost could go some way to overcoming these challenges. In addition to improvements in component performance and reliability, economy-of-scale improvements are necessary to achieve this reduction in cost [7]. This can be achieved by developing system components with a wide operating envelope, thus allowing the high-volume production of a single component that can be used in multiple applications. The focus of this paper is to investigate working-fluid replacement as a means of widening the operating envelope of small-scale ORC radial turbines. The focus on radial turbines is driven by the premise that they are a technically mature, compact, lightweight, robust and cheap technology. Furthermore, as heat-source temperatures rise the optimal pressure ratio across the expander increases, which limits the use of volumetric expanders such as scroll and screw technologies based on their low built-in volumetric ratios.

The use of organic fluids in turbines introduces additional complexities compared to designing conventional turbines for gas and steam applications. Firstly, organic fluids deviate from ideal gas law behaviour within the operating range typically experienced by an ORC turbine. Therefore, design and simulation models must be coupled with a suitable equation of state. Furthermore, organic fluids may also exhibit non-classical fluid dynamic behaviour where classical fluid dynamic effects are reversed [8–10]. The extent to which these effects are observed within ORC turbines is still not well understood, but is an active area of research, for example in Refs. [11–13]. Another complexity that arises from using an organic fluid in turbines is a low speed of sound, which means that supersonic conditions are experienced at lower isentropic enthalpy drops compared to conventional turbine designs. Most notably, supersonic conditions will be experienced within the stator, but could also be present in the rotor. For rotor inlet absolute Mach numbers only slightly exceeding unity, a choked converging stator can be designed, and the expansion to the design Mach number can be achieved in the rotor-stator interspace. For higher absolute Mach numbers, a converging-diverging stator is required. The design of the diverging section of the stator is critical, and in its simplest form is a supersonic nozzle which is geometrically manipulated to deliver the flow to the rotor inlet at the correct flow angle.

Aldo and Argrow [14] first developed a 2D axisymmetric minimum-length nozzle design model suitable for dense gases. This model used the method of characteristics and accounted for fluid properties using the van der Waals equation of state. Alternatively, Hoffren et al. [15] coupled an existing 2D ideal gas viscous flow solver to a real gas equation of state and studied the design of a supersonic stator operating with Toluene. The results were found to agree reasonable well with 1D design calculations. Other researchers have also used computational fluid dynamics (CFD) to investigate the performance of ORC supersonic stators [16–18]. Pasquale et al. [19] developed a more advanced stator design model, in which the the stator profile is optimised by coupling a CFD solver with a evolutionary algorithm. The objective was to optimise the stator geometry to minimise the total pressure loss whilst obtaining a uniform flow distribution at the stator outlet. Persico [20] also applied an evolutionary algorithm to optimise the design of a supersonic stator for organic vapours. Alternatively, the adjoint method has been studied for the same purpose [21], whilst Bufi and Cinnella [22] developed an optimisation strategy that considered a multi-objective optimisation of the average and variance of the stator isentropic efficiency. Wheeler and Ong [23] developed a stator design method based on the method of characteristics, and assumed that the working fluid obeys the polytropic relationship $P/\rho^k = \text{constant}$, where k is the polytropic index. This allowed the Prandtl-Meyer function ν to be formulated as a function of k. The nozzle designs that resulted from this model were validated using CFD, before being implemented within an ORC turbine stator. Later this design model was used to study unsteady effects in ORC turbines [24].

A major challenge facing numerical studies on ORC turbines is that of obtaining experimental data for validation of design models and CFD solvers. Currently, there are a few commissioned test facilities that aim to address this challenge [25–28]. Already there have been interesting results concerning trailing-edge losses in ORC turbines [27], and

experimental observations of the expansion of MDM within a converging-diverging nozzle [29]. These results, along with further developments in the other test facilities, will remain critical for the future validation of numerical models.

So far, the studies discussed concern the operation of a particular ORC stator, designed for a particular working fluid. Moreover, only a single design point is typically considered, although multi-point design methods have also been proposed [30]. However, to address concerns over high costs for small ORC systems, the authors believe it is necessary to investigate using the same turbine within various applications; this implies designing turbines for multiple design points, but also requires an understanding of how a turbine design responds to changes in the operating conditions or the working fluid. Previous work conducted by the authors has explored using a modified similitude model to scale a turbine's design point to alternative working fluids [31]. The application of the modified similitude theory to an ORC turbine leads to:

$$\left[\frac{\Delta h_\mathrm{s}}{N^2D^2},\, \eta\right] = f\left(\frac{\dot{m}}{\rho^* N D^3},\, \frac{ND}{a^*}\right), \tag{1}$$

where Δh_s is the turbine isentropic enthalpy drop, η is the turbine isentropic efficiency, $\dot{m}$ is the mass-flow rate, N is the rotational speed, D is the rotor diameter and a^* and ρ^* are the speed of sound and density at the choked stator throat. The first term on the left-hand side of the equation is the head coefficient, whilst the terms on the right-hand side are the flow coefficient and blade Mach number respectively. In the previous work [31], the predictions made using Equation 1 for $\dot{m}$ and η following a change in the working fluid were compared to CFD simulations and the results agreed to within 1%. Furthermore, it was shown that by changing the working fluid the same turbine could be used in different ORC systems, each designed for a different thermal input. However, this study was limited to rotor inlet absolute Mach numbers that only just exceeded unity since the stator had a simple converging geometry.

Other authors have studies the application of similitude theory to predict turbine performance following a change in working fluid [32–34]. However, missing from these studies is a detailed investigation into working-fluid replacement, accounting for supersonic flows and the presence of non-ideal gas effects. The aim of this paper is to extend the concept of working-fluid replacement to supersonic ORC turbines, with a view to moving towards modular ORC components that can be mass produced on a large scale and installed across a wide range of applications. Within this paper, focus is given to the stator since supersonic flows and non-ideal gas effects are more prevalent within the stator than within the rotor. After this introduction, two ORC systems are defined in Section 2 for R245fa and Toluene as working fluids. Then, in Section 3, a supersonic radial turbine stator is designed for each working fluid and these designs are validated using CFD in Section 4. The performance of these two stators following working-fluid replacement is then investigated in Section 5, whilst the implications on ORC system design are discussed in Section 6. The main findings from this research are summarised in Section 7.

2 Thermodynamic cycle and turbine design

Two ORC systems and two working fluids are considered in this study. R245fa is a common working fluid for low-temperature ORC applications [5, 35], whilst Toluene is a suitable candidate for high-temperature applications [7, 36]. A simple subcritical ORC is considered, albeit with operation close to the critical point; for both cycles the turbine inlet pressure is set to 95% of the critical pressure P_cr. Not only is operation close the critical point typical for supersonic ORC turbines, but also non-ideal gas effects are most prevalent near the critical point; this ensures these effects are accounted for within this study. The turbine inlet temperature is set to 101% of the critical temperature T_cr to ensure a suitable superheat to avoid two-phase conditions during expansion. The ORC thermodynamic design is completed by defining the condensation temperature T_cr. For the R245fa cycle, $T_\mathrm{c} = 323$ K is assumed to ensure a suitable condenser pinch point. For Toluene, the condensation pressure is set to 100 kPa to avoid sub-atmospheric operation, which corresponds to $T_\mathrm{c} = 383$ K. The pump and turbine efficiencies are set to 70% and 80% respectively. The resulting thermodynamic cycles are described in Tab. 1. The Toluene cycle is suitable for heat-source temperatures in excess of 600 K, whilst the R245fa cycle is suitable for heat-source temperatures around 450 K.

Table 1. Thermodynamic cycles and turbine designs

	R245fa	Toluene	
T_c	323.0	383.3	K
P_{01}/P_5	10.12	39.20	-
η_orc	12.94	17.21	%
T_{01}	431.4	597.7	K
P_{01}	3468	3920	kPa
$\dot{m}$	1.76	0.45	kg/s
N	47.4	88.1	kRPM
Ma_4	1.40	1.70	-
α_4	74.5	74.5	°
b_4	2.38	1.23	mm
P_4	1138	677	kPa
η_ts	83.2	83.2	%
k	0.80	0.85	-

To design the turbine, non-dimensional turbomachinery design parameters are used (Tab. 2), which are set to val-

Table 2. Turbomachinery design inputs

N_s	ν_{ts}	ψ	ϕ	r_5/r_4	r_4	ζ_n
0.55	0.68	0.90	0.25	0.55	40 mm	0.11

ues defined in the literature [37, 38]. Since the focus of this study is to investigate working-fluid replacement effects, rather than designing a turbine for a specific ORC application, the rotor inlet radius is set arbitrarily to 40 mm, and the mass-flow rate and power output are outputs from the turbine design process. The resulting turbine designs are also given in Tab. 1. The polytropic index k is calculated according to in Ref. [23]

The extent to which non-ideal gas dynamics are expected within the turbine is investigated in Fig. 1 by determining how the compressibility factor z, the fundamental derivative Γ, and the parameter J vary during an expansion from T_{01} and P_{01} to increasing values of Mach number, Ma. The compressibility factor is defined as:

$$z = \frac{P}{\rho RT}, \tag{2}$$

where P is the pressure, ρ is the density, R is the specific-gas constant and T is the temperature. The compressibility factor is a measure of how non-ideal a gas behaves at a specific operating point, with $z = 1$ corresponding to an ideal state. The fundamental derivative is defined as:

$$\Gamma = 1 + \frac{\rho}{a}\left(\frac{\partial a}{\partial \rho}\right)_s, \tag{3}$$

where a is the local speed of sound and s is the entropy. Finally, J is defined as:

$$J = 1 - \Gamma - \frac{1}{Ma^2}. \tag{4}$$

For a dense gas, $\Gamma < 1$, which corresponds to a reduction in the speed of sound through an expansion [8], whilst non-classical fluid dynamic effects are predicted when $J > 0$ [39]. From Fig. 1 it is observed that $\Gamma < 1$ but $J < 0$ during expansion up to $Ma = 2.5$. Therefore, for the expansion of Toluene or R245fa within a typical ORC turbine, conventional fluid dynamic effects are expected (*i.e.*, compression shocks and expansion fans). However, the fluid behaviour is still non-ideal with $0.5 < z < 1$ for both working fluids.

3 Supersonic stator design

A 2D minimum-length nozzle design model is used to design the supersonic part of an ORC turbine stator. This model is based on the method of characteristics (MoC) and is coupled to a real gas equation of state [40] to account for non-ideal

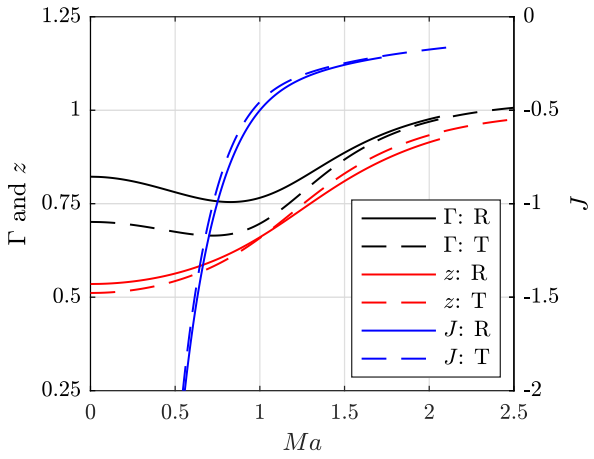

Fig. 1. Γ, z and J for expansion of R245fa and Toluene from $0.95P_{cr}$ and $1.01T_{cr}$ to increasing Mach numbers

fluid behaviour. The MoC model has been previously validated using CFD for the design of two converging-diverging nozzles operating with R245fa and Toluene with the same inlet conditions and Mach numbers as those given in Tab. 1 [41]. It was observed that the MoC model produces supersonic nozzles that expand the working fluids to the desired Mach number. However, weak oblique shocks were observed within the nozzle, which are attributed to the flow interaction with the nozzle wall boundary layers which reduce the effective nozzle flow area. The nozzle design could be improved by widening the nozzle passage to account for this boundary layer displacement, but since the outlet Mach numbers agree to within 1%, this further complication was deemed unnecessary.

Using the validated supersonic nozzle designs, the supersonic stators can be constructed. The purpose of this paper is not to complete a full optimisation of the stator design, but to investigate the effects of working-fluid replacement in ORC supersonic stators. Therefore, instead of implementing a sophisticated design optimisation model, similar to those reported in the Refs. [19,21], a stator design method has been developed that facilitates the quick generation of a stator geometry that is suitable for this investigation. A summary of the design method and the final stator designs is given in 7.

4 CFD simulation formulation and design validation

To validate the R245fa and Toluene stator designs, a steady-state CFD simulation was setup in ANSYS CFX, which solves the full 3D Navier-Stokes equations using the finite-volume method. Since this analysis is considering only the stator vane a steady-state simulation is suitable, although the importance of using unsteady simulations to simulate the interaction between stator trailing-edge shocks and the rotor leading edge has been discussed [24,42]. Therefore this analysis takes no account of shock reflections from the rotor, although this should be one focus of future studies. Two quasi-2D meshes were constructed using Turbogrid, with only one element in the z-direction and a symmetry plane was applied.

The inlet conditions were set to the turbine total inlet conditions. The radius of the CFD outlet domain was set to 38 mm rather than setting it to the rotor inlet radius (r_4 = 40 mm) to ensure the outlet domain is sufficiently downstream of the trailing-edge wake such that the wake is fully mixed out before it reaches the boundary. The outlet boundary conditions were set to the average static pressure, with the pressure profile blend set to 5%. The outlet pressures were estimated by applying a 1D mass, energy and momentum balance between the rotor inlet radius and the radius of the CFD outlet domain. This corresponded to outlet pressures of 1000 kPa and 550 kPa for the R245fa and Toluene nozzles respectively. The k-ω SST turbulence model with automatic wall function was selected, and the high-resolution scheme was used for both the advection and turbulence calculations. To account for non-ideal fluid properties, REFPROP was used to generate fluid property look-up tables which are accessed by CFX during the simulations. During previous studies it has been found that a table size of 100×100 is sufficient, with the change in the nozzle loss coefficient predicted by this table size compared to a table size of 250×250, being less than 0.1% [41]. The grid-independent meshes used for the R245fa and Toluene stators were both constructed from 1.4×10^5 elements; an example of the mesh is shown in Fig. 2.

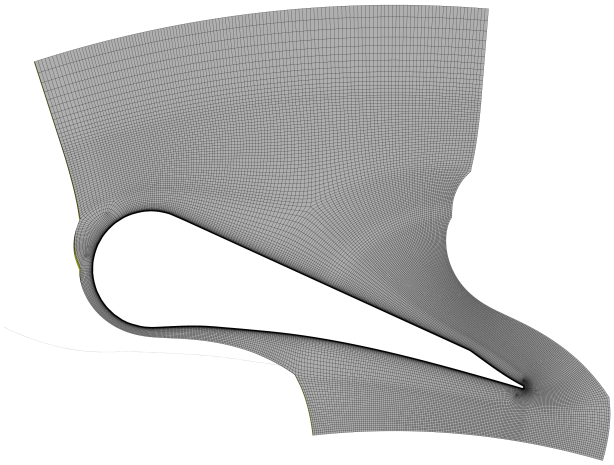

Fig. 2. Stator mesh consisting of 1.4×10^5 elements

The Mach number contours predicted by the CFD simulations for the two stators are shown in Figs. 3 and 4, whilst the Mach number distributions along the nozzle centreline are shown in the top plot in Fig. 5. It is apparent that the flow is expanded within the diverging part of the supersonic nozzle to the desired Mach number for both stator designs. Downstream of the diverging section a more complex flow pattern is observed for both stators. This is the consequence of the generation of shockwaves at the trailing edge, and the interaction of these shocks with the boundary layer that develops on the stator blade walls. This shockwave-boundary layer interaction leads to an uneven distribution in the centreline Mach number downstream of the stator trailing edge, as observed in Fig. 5 for normalised streamwise locations greater than 0.7. This figure also displays the local loss coefficient at the rotor inlet radius, which is defined as:

$$\xi = \frac{h - h_s}{h_{01} - h_{4s}}, \tag{5}$$

where h and h_s are the local enthalpy and local isentropic enthalpy respectively, h_{01} is the total inlet enthalpy and h_{4s} is the mass-averaged isentropic enthalpy across the whole rotor inlet. The greatest source of loss for both nozzles is in the wake generated downstream of the stator trailing edge, whilst a second source of loss is associated with the trailing-edge shocks observed at a normalised pitch of 0.95.

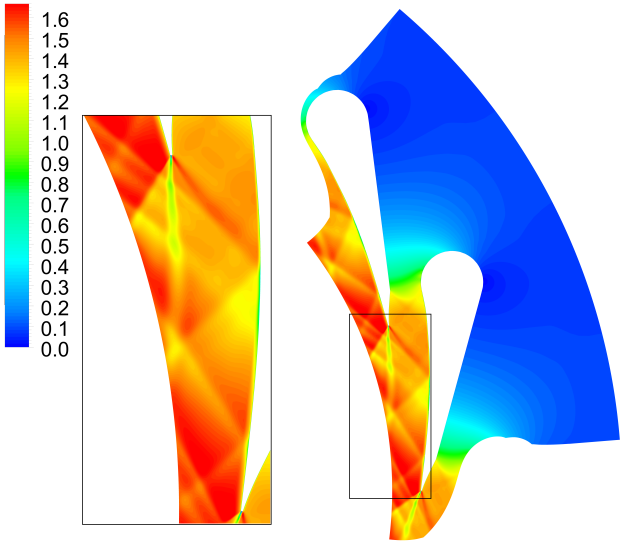

Fig. 3. Contours of absolute Mach number predicted by CFD for the R245fa supersonic stator vane

The overall performance of both stators is evaluated by calculating the overall stator loss coefficient ζ_n, which is based on the mass-averaged static outlet conditions at the rotor inlet radius:

$$\zeta_n = \frac{h_4 - h_{4s}}{\frac{1}{2}c_4^2}. \tag{6}$$

The loss coefficients are 0.0672 and 0.0449 for the R245fa and Toluene stators respectively, which are both lower than the value specified for the preliminary design (Tab. 2). Since the R245fa stator expands to a lower Mach number than the Toluene stators, this implies the larger loss is the result of a wider and deeper wake, rather than being associated with increased shock losses. This can be observed in Figs. 3 and 4, and is further confirmed by comparing the loss profiles in Fig. 5. It is worth noting that ζ_n has been evaluated at the rotor inlet radius, where the flow is not fully mixed-out. Therefore, the calculation was repeated further

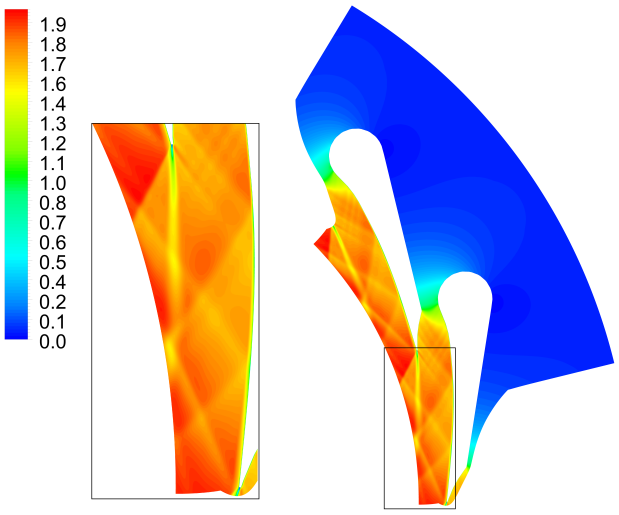

Fig. 4. Contours of absolute Mach number predicted by CFD for the Toluene supersonic stator vane

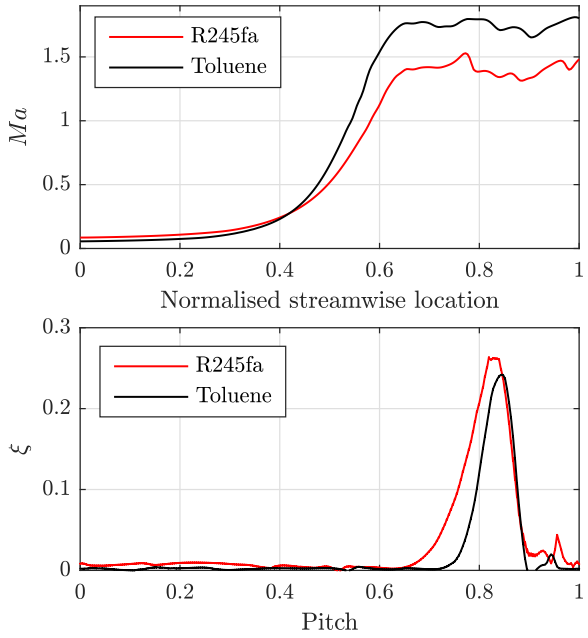

Fig. 5. CFD results for the R245fa and Toluene supersonic stators: stator centreline Mach number (top); local loss coefficient at rotor inlet radius (r_4 = 40 mm) (bottom).

downstream, at a radius of 39 mm. At this location, the flow is more mixed-out, but it was found that the change in the loss coefficients was negligible.

Based on the area-averaged velocity components obtained from the CFD simulations, and the rotational speeds defined in Tab. 1, the velocity triangles at the rotor inlet can be constructed (Fig. 6). The absolute flow angles α_4 predicted by CFD for the R245fa and Toluene stators are 75.4° and 76.0° respectively, which are higher than the design value of 74.5°. The causes a shift in the velocity triangle, and a reduction in the relative flow angle. The mass-flow rates predicted from the CFD simulations are 1.74 kg/s and

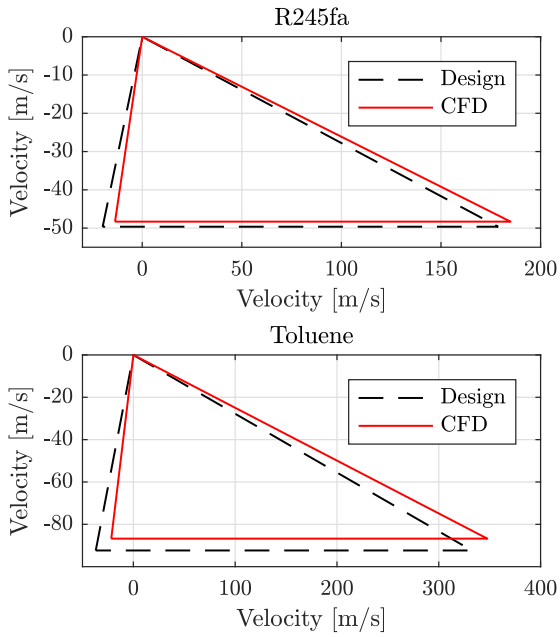

Fig. 6. Comparison of the design point rotor inlet velocity triangles with the area-averaged rotor inlet velocity triangles obtained from the CFD simulations for the R245fa (top) and Toluene (bottom) stators

0.44 kg/s for the R245fa and Toluene stators respectively. These are slightly less than the design values and correspond to percentage reductions of 1.2% and 3.3%. This reduction may be due to boundary-layer blockage effects, which reduce the effective throat width, thereby reducing the mass-flow rate that can pass through the stator. Referring to Tab. 4, the design point throat Reynolds numbers for the R245fa and Toluene stators are 2.52×10^6 and 1.09×10^6 respectively. Therefore, these results are consistent with boundary layer theory, which would predict a reducing boundary layer displacement thickness with increasing Reynolds number.

Overall, the stator designs achieve conditions that are close to the desired flow conditions at the rotor inlet. Further refinement and optimisation could improve the stator performance further, which may include adapting the MoC model to account for boundary layer blockage, increasing the number of stator vanes to reduce the loss coefficient [23], or using advanced optimisation methods to improve the stator blade profile [19, 21]. However, this was not one of the objectives of this study. It should also be noted that since these were quasi-2D simulations, no consideration has been given to end-wall effects, and particularly the end-wall boundary layers which would further reduce the mass-flow rate and stator loss coefficient. Further studies should take these effects into account.

5 Scaling of the stator design point

Having verified the performance of both stators at the design point, it is now possible to study the effects of working-fluid replacement. In the previous study [41] that investigated working-fluid replacement in a simple converging-diverging

nozzle, it was suggested that by conserving the amount of flow turning within the nozzle (*i.e.*, the Prandtl-Meyer function, ν), the nozzle design point could be scaled to alternative working fluids. To expand on this idea, ν is plotted in Fig. 7 for the expansion of R245fa from $0.95P_{cr}$, $0.70P_{cr}$ and $0.45P_{cr}$ to a range of different Mach numbers. As observed, expansion from a lower pressure results in reduced flow turning for expansion to the same Mach number. Therefore, it is suggested that by assuming that ν remains constant, the outlet Mach number following a change in working fluid or inlet conditions can be predicted through interpolation of the data in Fig. 7. However, in the previous study [41] this method was only accurate when there was no significant change in the polytropic index k. More specifically, predictions made by conserving ν agreed with the CFD results to within 2%, provided that $0.9 < k/k_d < 1.1$, where k_d is polytropic index associated with the original design point. This suggests that using the same stator with different working fluids will only be possible if the two fluids undergo a similar change in density (*i.e.*, ρ/ρ_0) during an isentropic expansion across a defined pressure ratio (P/P_0). Furthermore, considering that ν can be approximated by an expression that is a function of Ma and k [23], it follows that if a working fluid and the total inlet conditions could be appropriately selected to conserve ν and k, the performance of the nozzle and the nozzle outlet Mach number would be the same.

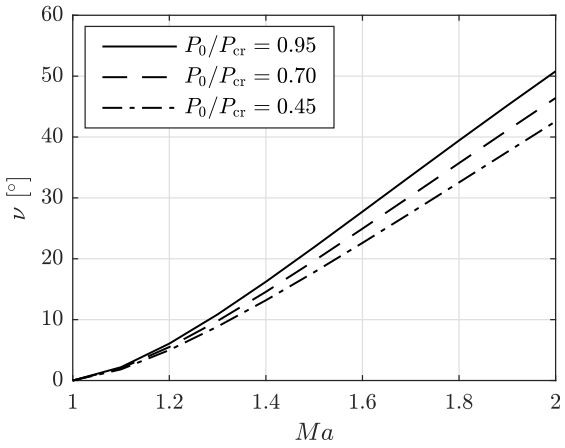

Fig. 7. Variation in ν for the expansion of R245fa from different total inlet pressures to a range of Mach numbers Ma

The relationship between k and the total inlet conditions is explored in Fig. 8, for a number of common organic working fluids. For each working fluid an isentrope is constructed that starts at $0.95P_c$ and $1.01T_c$. For different total inlet pressures along this isentrope the outlet Mach number and corresponding static outlet pressure are selected to ensure the same value for ν that is associated with either the R245fa or Toluene stator design. The ratios P/P_0 and ρ/ρ_0 are then determined for an array of pressures ranging from the inlet pressure to the outlet pressure, and k is determined using a linear regression. The results shown in Fig. 8 are normalised by the design point polytropic index k_d.

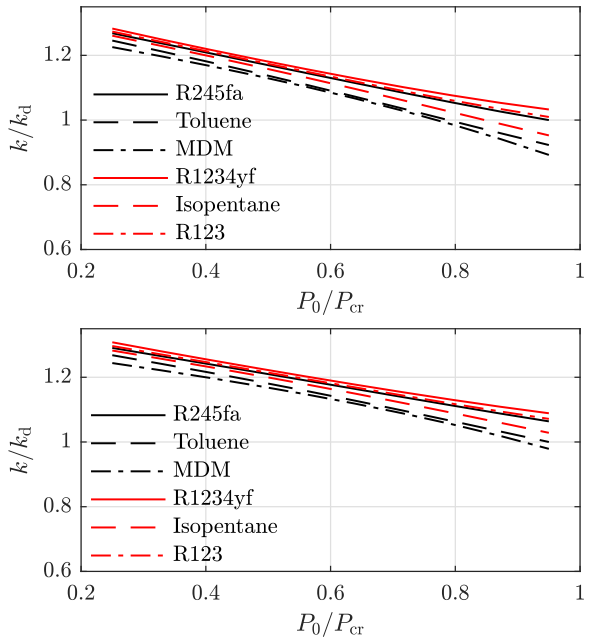

Fig. 8. The variation in the normalised polytropic index k/k_d for the expansion of different working fluids from different reduced total inlet pressures P_0/P_{cr}. For each case the static outlet conditions are selected to maintain the same Prandtl-Meyer function ν that is associated with the original design point: R245fa stator (top); Toluene stator (bottom).

The results from Fig. 8 can be used as a basis for scaling the two stator design points to alternative working fluids. For the six working fluids considered, the total inlet conditions and static outlet pressure at the CFD outlet radius (38 mm) are selected to ensure that ν is conserved, and that the ratio $k/k_d \approx 1$. The resulting scaled design points for the two stators are given in Tab. 3. During this scaling, the expansion process is assumed to be isentropic and therefore there is no consideration of any shock or viscous losses within the stator; hence, the scaling process is an oversimplification as these effects will undoubtably be present within ORC turbines. However, providing that the stator nozzle is performing at the design point any shockwaves present will at the stator trailing edge. Moreover, viscous losses are confined to the stator blade wall, causing an effective reduction in the passage area, but not an increase the freestream entropy. Therefore, the isentropic assumption should be valid for the flow conditions within the stator passage. However, if this is found to be an oversimplication, this assumption will be refined in future studies.

The deviation in the Reynolds number ranges between $0.47Re_d$ and $1.03Re_d$ for the R245fa stator, and $0.71Re_d$ and $1.35Re_d$ for the Toluene stator. These deviations are within the acceptable range previously determined ($0.5 < Re/Re_d < 2$) [41], and therefore Reynolds number effects are not expected to be significant. When considering the R245fa stator

Table 3. Stator inlet conditions and static outlet pressures for the alternative working fluid studies on the R245fa and Toluene stators

	R245fa stator					Toluene stator				
	T_{01}	P_{01}	P_4	$\frac{Re}{Re_d}$	$\frac{k}{k_d}$	T_{01}	P_{01}	P_4	$\frac{Re}{Re_d}$	$\frac{k}{k_d}$
	K	MPa	MPa			K	MPa	MPa		
R245fa	431	3.47	1.00	1.00	1.00	431	3.47	0.45	1.30	1.06
Toluene	586	3.28	0.94	0.68	1.00	598	3.92	0.55	1.00	1.00
MDM	564	1.10	0.31	0.47	1.00	568	1.30	0.18	0.71	1.00
R1234yf	372	3.21	0.92	1.03	1.03	372	3.21	0.40	1.35	1.08
Isopentane	459	2.89	0.82	0.79	1.00	465	3.21	0.43	1.11	1.03
R123	461	3.48	1.00	0.99	1.01	461	3.48	0.44	1.29	1.06

it is possible to select a suitable total inlet condition that conserves k for all working fluids except R1234yf, as is evident from Fig. 8. However, for the Toluene nozzle this is only possible for MDM. Therefore, for R245fa, R1234yf, Isopentane and R123, the total conditions are set to $0.95P_{cr}$ and $1.01T_{cr}$, and this corresponds to maximum deviations in k that are between 3% and 6%.

For each working fluid, two CFD simulations are performed to assess the performance of the R245fa and Toluene stators with that working fluid. Then, for each combination of stator and working fluid, the midline Mach number distribution, the loss profile at the rotor inlet radius, and the overall stator loss coefficient were obtained. The Mach number distributions and loss profiles are shown in Figs. 9 and 10 respectively. From these figures, it is clear that for the cases given in Tab. 3 the performance of both stators remains the same. This indicates that the method employed has successfully scaled the stator design point to the alternative fluids.

The values for ζ_n calculated from the CFD simulations range between 0.0672 and 0.0582 for the R245fa stator, operating with R245fa and MDM respectively, and range between 0.0471 and 0.0449 for the Toluene stator, when operating with R245fa and Toluene respectively. Similarly, for the R245fa stator, α_4 ranges between 75.3° and 75.4° for MDM and Toluene, whilst for the Toluene stator α_4 ranges between 75.7° and 76.0° for R123 and Toluene. The mass-flow rates range between 0.58 kg/s and 1.82 kg/s for the R245fa stator, and 0.22 kg/s and 0.58 kg/s for the Toluene stator.

Overall, the CFD results obtained for the two stators operating with alternative fluids have shown that the performance of the stator remains the same, provided that the change in k is not significant. Under this condition the stator performance can be predicted by conserving ν.

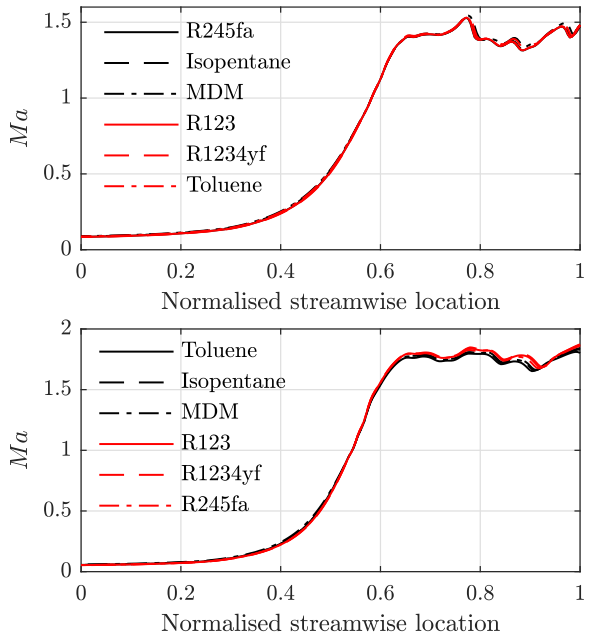

Fig. 9. Midline Mach number distributions for the two stators operating with alternative working fluids: R245fa (top); Toluene (bottom).

6 Implementation within practical ORC systems

To conclude this paper it is necessary to consider the practical ORC systems in which working-fluid replacement could be used for beneficial effect. Similitude theory hypothesises that the non-dimensional performance of a turbine is the same when the Mach number velocity triangles at the rotor inlet and outlet are the same. Therefore, considering the similarities in the Mach numbers and absolute flow angles at the rotor inlet predicted by the CFD simulations, the rotor blade velocity u_4 can be selected to ensure the same relative flow angle, and relative Mach number at the rotor inlet; note that the subscripts '4' and '5' refer to the rotor inlet and rotor outlet respectively, following on from the convention where '1', '2' and '3' refer to the turbine inlet, stator leading edge and stator trailing edge respectively.

Once u_4 is known, a suitable method for predicting the rotor outlet conditions is required. Unlike the stator, for which a scaling method based on the Prandtl-Meyer function has been developed within this paper, it is assumed that conventional turbomachinery design methods can be used to scale the rotor. The reasoning behind this is that generally the flow conditions within the rotor will remain subsonic, and

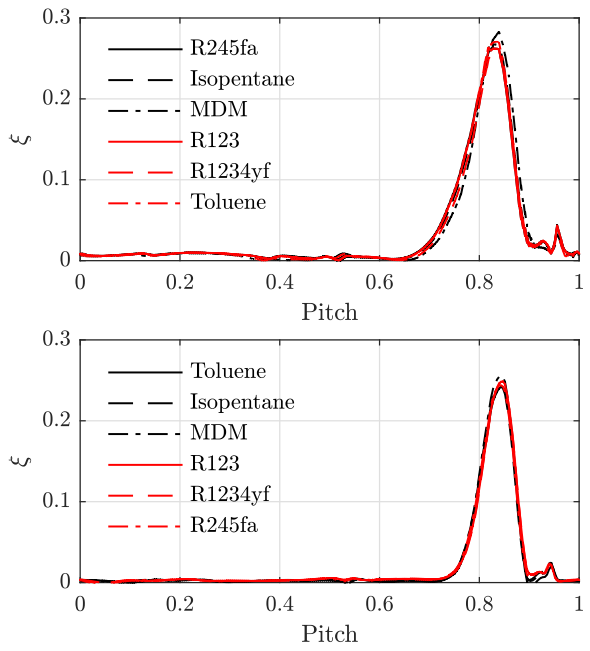

Fig. 10. Local loss coefficient at r_4 for the two stators operating with alternative working fluids: R245fa (top); Toluene (bottom).

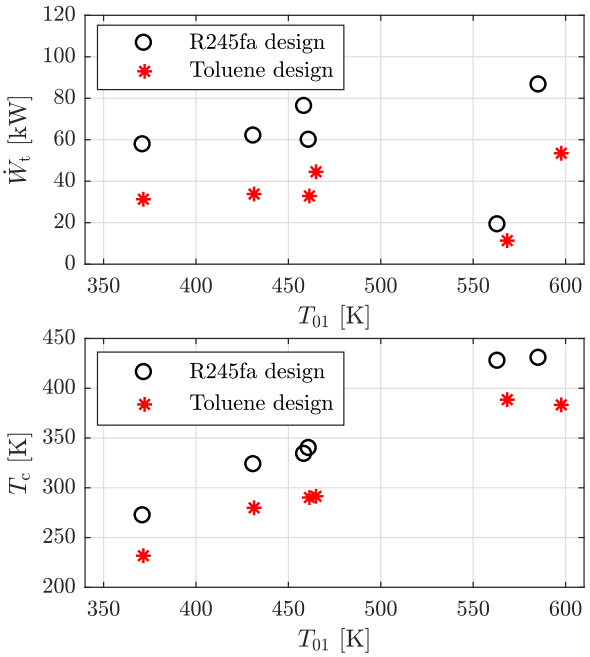

Fig. 11. Turbine power (top) and ORC condensation temperatures (bottom) for the R245fa and Toluene turbines when operating with alternative working fluids at different turbine inlet temperatures

therefore the complexity of requiring similar scaling methods based on the Prandtl-Meyer number is removed. Moreover, the flow conditions within the rotor are further away from the critical point, and therefore non-ideal gas effects will be less prevalent. Based on this assumption, u_4 can be related to the isentropic static enthalpy at the rotor outlet h_{5s} by assuming the rotor operates at the design point isentropic velocity ratio ν_{ts}, hence:

$$h_{5s} = h_{01} - \frac{1}{2}c_s^2 = h_{01} - \frac{1}{2}\left(\frac{u_4}{\nu_{ts}}\right)^2. \tag{7}$$

This allows the turbine static outlet pressure P_5 to be determined, from which the total-to-static pressure ratio (P_{01}/P_5) is also known. Finally, assuming that the rotor operates at the design isentropic velocity ratio implies the same total-to-static isentropic efficiency η_{ts}, which allows the turbine power to be estimated:

$$\dot{W}_t = \dot{m}\eta_{ts}(h_{01} - h_{5s}). \tag{8}$$

The results from this analysis are shown in the top plot of Fig. 11, and these suggest that operating the R245fa turbine with alternative working fluids could allow the same turbine to be used within different ORC systems with T_{01} ranging between 372 K and 586 K, and $\dot{W}_t$ ranging between 18.9 kW and 86.3 kW. Similarly, operating the Toluene turbine with alternative fluids could facilitate the use of the same turbine within ORC systems with T_{01} ranging between 372 K and 598 K, and $\dot{W}_t$ ranging between 11.4 kW and 53.5 kW.

At first glance these results suggest the feasibility of using the turbine within multiple ORC systems, thus facilitating economy-of-scale improvements. However, it is also necessary to consider the resulting ORC condensation temperatures T_c, which can be obtained from P_5 and are given in the bottom plot in Fig. 11. When evaluating these results it becomes apparent that not all of the ORC systems will be practical. For example, the Toluene turbine couldn't be used with R1234yf, R245fa, R123 and Isopentane because these working fluids result in condensation temperatures below 300 K, which could not be achieved without a very low-temperature heat sink. In comparison, the R245fa turbine could be used with all the fluids with the exception of R1234yf, since T_c for these cases are all above 300 K. From the plot in the bottom half of Fig. 11 it is also apparent that a relationship between increasing T_{01} and increasing T_c exists. This echoes the relationship between the critical temperature and the normal boiling point that has been shown within the literature [43]. Therefore, given that the critical temperature of Toluene is greater than R1234yf, R245fa, R123 and Isopentane, whilst R245fa has the second lowest critical temperature after R1234yf, this suggests that a supersonic turbine design cannot be scaled to a working fluid with a lower critical temperature, as this will result in a low condensation temperature and an infeasible ORC system.

Whilst the Toluene design cannot be used with working fluids that have lower critical temperatures than that of Toluene, opportunities remain to improve the economy-of-scale of small ORC systems by replacing the working fluid in the R245fa turbine. To explore this, the analysis has been extended to a wider group of working fluids, all with critical temperatures greater than R245fa. For each working

fluid, T_{01}, P_{01} and P_4 were determined to conserve both k and ν within the stator. The flow angles α_4 and β_4 were assumed constant and P_5 was determined from Equation 7. The mass-flow rate is determined from the reduced flow coefficient $\dot{m}/(\rho^* a^*)$, which is assumed constant since the stator geometry does not change. This, in turn, determines $\dot{W}_t$ if it is assumed that η_{ts} is constant; such an assumption can be made since similitude theory hypothesises that the turbine performance will be the same if the rotor velocity triangles and flow coefficient are maintained. The results from this analysis are shown in Fig. 12.

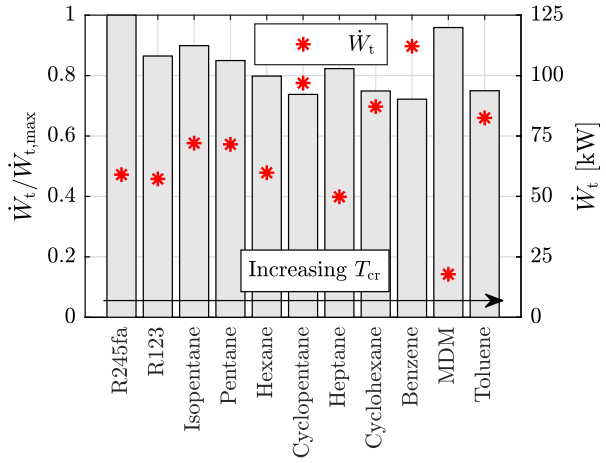

Fig. 12. Power produced from the R245fa turbine when the design point is scaled to alternative working fluids

In Fig. 12, $\dot{W}_t$ has been normalised by the maximum power $\dot{W}_{t,max}$. This is done because within the scaling process the designer has no control over P_5, and therefore a high condensation temperature could result which would have a detrimental effect on the ORC performance. The maximum power is calculated by assuming that the working fluid is expanded from the same total inlet conditions to the minimum permissible condensation temperature. The minimum condensation temperature depends on the availability and temperature of the heat sink, and the size of the ORC condenser, which affect the minimum temperature difference within the condenser. For this analysis, a value of 323 K is assumed to be a reasonable value. For working fluids that have a sub-atmospheric condensation pressure at 323 K, the minimum condensation temperature is increased to the saturation temperature at 100 kPa to avoid sub-atmospheric condensation. The mass-flow rate for the maximum power case is determined by assuming that the same amount of thermal energy is available to the ORC system in both cases.

From Fig. 12, it is observed that $\dot{W}_t$ ranges between 17.8 kW for MDM and 112 kW for Benzene. Furthermore, the results have been plotted in order of increasing critical temperature, and therefore correspond to ORC systems that are suitable for different heat-source temperatures. This highlights the possibility of using the same turbine within different ORC systems by matching the working fluid to the available heat source. MDM and Benzene also correspond to the maximum and minimum values for the normalised power, with values of 0.96 and 0.72 respectively, suggesting there could be up to a 30% reduction in the normalised power output following working-fluid replacement, compared to a system with an optimised condensation pressure.

A relationship between P_{01} and the normalised power is also observed (Fig. 13), with lower inlet pressures corresponding to higher normalised powers. This trend is even clearer when the working fluids are divided by how the optimised condensation temperature is determined (*i.e.*, $T_c =$ 323 K, or defined by the saturation temperature at 100 kPa). A correlation is also observed between a higher normalised power and a condensation temperature that is closer to the minimum permissible condensation temperature. For example, for the MDM system, which has the highest normalised power, the condensation temperature is 431.5 K, whilst the condensation temperature at 1 bar is 425.2 K. For the Benzene system, which has the lowest normalised power, the condensation temperature is 411.1 K, compared to a condensation temperature at 1 bar of 352.8 K. The corresponding condensation pressures for these two working fluids are 117 and 425 kPa respectively. In other words, using the R245fa turbine with Benzene would lead to an under expansion of the working fluid, compared to an optimal cycle in which the fluid is expanded down to 100 kPa. The cycle efficiencies for the scaled cycles range between 8.1% (MDM) and 15.7% (cyclopentane), compared to 8.5% and 21.3% for the same working fluids, but with expansion down to the minimum permissible condensation temperature.

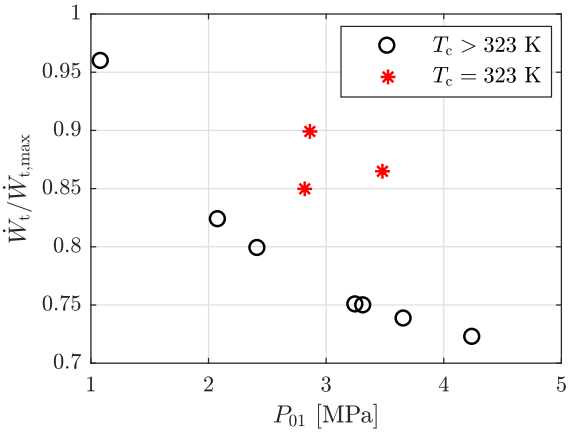

Fig. 13. Relationship between the normalised power produced from the R245fa turbine when operating with different working fluids and the turbine inlet pressure P_{01}. The results are split into two groups: (i) $T_c = 323$ K, and (ii) saturation temperature at 100 kPa (*i.e.*, $T_c >$ 323 K).

At this stage a link to the authors' previous work, which applied similitude theory to subsonic ORC radial turbines [44], can be made. In this work, it was shown that the performance of a subsonic radial turbine can be predicted based

on the reduced head coefficient $\Delta h_s/a^{*^2}$, reduced flow coefficient $\dot{m}/\rho^* a^*$ and reduced rotational speed N/a^*. From the CFD results presented in Section 5, it was found that the reduced flow coefficients equalled 1.12×10^{-4} and 3.59×10^{-5} for the R245fa and Toluene stators. This was to be expected since the stator geometry does not change. However, by conserving both ν and k when changing the working fluid we have conserved the Mach number triangles which means that the reduced head coefficient and the reduced rotational speeds also remain the same. For the results for the R245fa turbine shown in Fig. 12, the reduced head coefficients range between 3.10 and 3.13, which corresponds to a deviation of less than 1%. This small deviation arises because it was not always possible to select an operating point that conserved k (*i.e.*, Fig. 8). Nonetheless, these results suggest that the modified similitude theory is suitable for supersonic turbines, so long as k and ν do not deviate significantly.

The scaled rotor rotational speed ranges between 44 and 71 kRPM, which correspond to operating with R123 and cyclopentane respectively. This speed range is well within the practical limits for a rotor diameter of 80 mm. Therefore, the main practical constraint on using the same turbine with multiple working fluids is the variation in shaft power, which could require a different generator. However, even if a different generator is required, it is still envisioned that the same turbine assembly can be used, thereby removing the need to develop a new bespoke turbine design.

In summary, this section has demonstrated how a supersonic turbine design can be scaled to an alternative working fluid. However, the scaling process is subject to constraints which are imposed by the properties of the original and replacement working fluids, namely $0.9 < k/k_d < 1.1$ and $T_{cr} > T_{cr,d}$, which narrows the potential operational envelope of a particular turbine design. Nonetheless, the results suggest that through the careful selection of a replacement working fluid, the same ORC turbine could be suitable for different applications. However, this is not a one size fits all approach, as the effect of working-fluid replacement on the condensation pressure, and the possible reduction in the power output compared to an optimised thermodynamic cycle needs to be considered. In this instance, there is a trade-off between minimising the development and manufacturing costs of the turbine by using an existing design, but accepting a slight reduction in performance, and developing a bespoke design with optimal performance, but with higher associated costs. To answer this question a thorough economic assessment of the two options should be conducted.

Before concluding, a number of issues which require further investigation should be discussed. Firstly, it is reiterated that the stator designs have been obtained using a simple geometrical construction, and as such have not been optimised using advanced design techniques which are becoming more routinely used. Thus, further verification is required for an optimised stator design. Furthermore, the results have been obtained using simple assumptions pertaining to the rotor design. Therefore, further research efforts must also focus on a more detailed 3D rotor design phase, complemented with 3D CFD simulations of the complete stator and rotor assembly. With this in place, the effects of working-fluid replacement in supersonic ORC turbines can be studied in further detail. Finally, following from Refs. [24, 42], unsteady CFD simulations will also be necessary to investigate the role of unsteady effects on working-fluid replacement.

7 Conclusions

The effect of working-fluid replacement as a means of widening the operating envelope of a particular ORC supersonic turbine has been studied in this paper. Supersonic stators have been designed for R245fa and Toluene, and their design point performance verified using quasi-2D CFD simulations completed using ANSYS CFX. The design point for each stator was then scaled to alternative working fluids by conserving the Prandtl-Meyer function and the polytropic index. The CFD results show that provided the Prandtl-Meyer function and the polytropic index can be conserved, the centreline Mach number distribution and rotor inlet loss profile remain the same. Furthermore, the stator loss coefficients for the R245fa stator ranged between 0.0672 and 0.0582, whilst for the Toluene stator they ranged between 0.0471 and 0.449. The rotor inlet flow angles changed by less than 0.3° for both stators, further confirming that the design point has been accurately scaled to alternative working fluids.

Studies concerning the ORC system show that working-fluid replacement could facilitate using the same turbine in different applications. For example, the R245fa design could be used within ORC systems with maximum temperatures ranging between 431 K (R245fa) and 585 K (Toluene), whilst the power output could range between 17 kW (MDM) and 112 kW (Benzene). This suggests the potential to match the working fluid to the heat-source temperature and thermal content, whilst using the same turbine design. However, it is observed that working-fluid replacement may only be possible if the replacement working fluid has a higher critical temperature than the design working fluid. Furthermore, depending on the working fluid there could be up to a 30% reduction in the power output compared to an ORC system that is designed specifically for the new heat source. Nonetheless, from the point of view of turbine economy-of-scale improvements, working-fluid replacement could be used to beneficial effect. Future work should study the effects of working-fluid replacement on the full 3D flow within ORC supersonic turbines, and validate these ideas experimentally.

Acknowledgements

This work was supported by the UK Engineering and Physical Sciences Research Council (EPSRC) [grant numbers: EP/P004709/1 and EP/P009131/1].

References

[1] Markides, C. N., 2013. "The role of pumped and waste heat technologies in a high-efficiency sustainable energy future for the uk". *Appl Therm Eng,* **53**(2), pp. 197–209.

[2] Markides, C. N., 2015. "Low-concentration solar-power systems based on organic Rankine cycles for distributed-scale applications: Overview and further developments". *Frontiers in Energy Research,* **3**(December), pp. 1–16.

[3] Qiu, G., Shao, Y., Li, J., Liu, H., and Riffat, S. B., 2012. "Experimental investigation of a biomass-fired ORC-based micro-CHP for domestic applications". *Fuel,* **96**, pp. 374–382.

[4] Freeman, J., Hellgardt, K., and Markides, C. N., 2015. "An assessment of solar-powered organic Rankine cycle systems for combined heating and power in UK domestic applications". *Appl Energ,* **138**, pp. 605–620.

[5] Freeman, J., Hellgardt, K., and Markides, C. N., 2017. "Working fluid selection and electrical performance optimisation of a domestic solar-ORC combined heat and power system for year-round operating in the UK". *Appl Energ,* **186**, pp. 291–303.

[6] Lang, W., Colonna, P., and Almbauer, R., 2013. "Assessment of waste heat recovery from a heavy-duty truck engine by means of an ORC turbogenerator". *J Eng Gas Turb Power,* **135**(4).

[7] Colonna, P., Casati, E., Trapp, C., Mathijssen, T., Larjola, J., Turunen-Saaresti, T., and Uusitalo, A., 2015. "Organic Rankine cycle power systems: From the concept to current technology, applications, and an outlook to the future". *J Eng Gas Turb Power,* **137**(10).

[8] Thompson, P. A., 1971. "A fundamental derivative in gas dynamics". *Phys Fluids,* **14**(9), pp. 1843–1849.

[9] Colonna, P., and Guardone, A., 2006. "Molecular interpretation of nonclassical gas dynamics of dense vapors under the van der Waals model". *Phys Fluids,* **18**(5).

[10] Kluwick, A., 2017. "Non-ideal compressible fluid dynamics: A challenge for theory". *J Phys Conf Ser,* **821**.

[11] Mathijssen, T., Gallo, M., Casati, E., Nannan, N. R., Zamfirescu, C., Guardone, A., and Colonna, P., 2015. "The flexible asymmetric shock tube (FAST): A Ludwieg tube facility for wave propagation measurements in high-temperature vapours of organic fluids". *Experiments in Fluids,* **56**(195).

[12] Gori, V., Vimercati, D., and Guardone, A., 2017. "Non-ideal compressible-fluid effects in oblique shock waves". *J Phys Conf Ser,* **821**.

[13] Alferez, N., and Touber, E., 2017. "Shock-induced energy transfers in dense gases". *J Phys Conf Ser,* **821**.

[14] Aldo, A. C., and Argrow, B. M., 1995. "Supersonic minimum length nozzle design for dense gases". *J Fluid Eng,* **115**(2), pp. 270–276.

[15] Hoffren, J., Talonpoika, T., Larjola, J., and Siikonen, T., 2002. "Numerical simulation of real-gas flow in a supersonic turbine nozzle ring". *J Eng Gas Turb Power,* **124**(4), pp. 395–403.

[16] Colonna, P., Rebay, S., Harinck, J., and Guardone, A., 2006. "Real-gas effects in ORC turbine flow simulations: Influence of thermodynamic models on flow fields and performance parameters". In European Conference on Computational Fluid Dynamics.

[17] Harinck, J., Turunen-Saaresti, T., Colonna, P., Rebay, S., and van Buijtenen, J., 2010. "Computational study of a high-expansion ratio radial organic Rankine cycle turbine stator". *J Eng Gas Turb Power,* **132**(5).

[18] Harinck, J., Pasquale, D., Pecnik, R., Buijtenen, J. V., and Colonna, P., 2013. "Performance improvement of a radial organic Rankine cycle turbine by means of automated computational fluid dynamic design". *P I Mech Eng A-J Pow,* **227**(6), pp. 637–645.

[19] Pasquale, D., Ghidoni, A., and Rebay, S., 2013. "Shape optimization of an organic Rankine cycle radial turbine nozzle". *J Eng Gas Turb Power,* **135**(4).

[20] Persico, G., 2017. "Evolutionary optimization of centrifugal nozzles for organic vapours". *J Phys Conf Ser,* **821**.

[21] Pini, M., Persico, G., Pasquale, D., and Rebay, S., 2015. "Adjoint method for shape optimization in real-gas flow applications". *J Eng Gas Turb Power,* **137**(3).

[22] Bufi, E. A., and Cinnella, P., 2017. "Robust optimization of supersonic ORC nozzle guide vanes". *J Phys Conf Ser,* **821**.

[23] Wheeler, A. P. S., and Ong, J., 2013. "The role of dense gas dynamics on organic Rankine cycle turbine performance". *J Eng Gas Turb Power,* **135**(10).

[24] Wheeler, A. P. S., and Ong, J., 2014. "A study of the three-dimensional unsteady real-gas flows within a transonic ORC turbine". In Proceedings of the ASME Turbo Expo 2014, no. GT2014-25475.

[25] Spinelli, A., Pini, M., Dossena, V., Gaetani, P., and Casella, F., 2013. "Design, simulation, and construction of a test rig for organic vapors". *J Eng Gas Turb Power,* **135**(4).

[26] Reinker, F., Hasselmann, K., aus der Wiesche, S., and Kenig, E. Y., 2016. "Thermodynamics and fluid mechanics of a closed blade cascade wind tunnel for organic vapors". *J Eng Gas Turb Power,* **138**(5).

[27] Durá Galiana, F. J., Wheeler, A. P., and Ong, J., 2016. "A study of trailing-edge losses in organic Rankine cycle turbines". *J Turbomach,* **138**(12).

[28] Head, A. J., Servi, C. D., Casati, E., Pini, M., and Colonna, P., 2016. "Preliminary design of the ORCHID: A facility for studying non-ideal compressible fluid dynamics and testing ORC expanders". In Proceedings of ASME Turbo Expo 2016, no. GT2016-56103.

[29] Spinelli, A., Cozzi, F., Dossena, V., Gaetani, P., Zocca, M., and Guardone, A., 2016. "Experimental investigation of a non-ideal expansion flow of siloxane vapor MDM". In Proceedings of ASME Turbo Expo 2016, no. GT2016-57357.

[30] Macchi, E., and Astolfi, M., 2017. *Organic Rankine Cycle (ORC) Power Systems*. Woodhead Publishing.

[31] White, M., and Sayma, A. I., 2016. "Investigating the effect of changing the working fluid on the three-dimensional flow within organic Rankine cycle turbines". In Proceedings of ASME Turbo Expo 2016, no. GT2016-56106.

[32] Wong, C. S., and Krumdieck, S., 2016. "Scaling of gas turbine from air to refrigerants for organic Rankine

cycle using similarity concept". *J Eng Gas Turb Power,* **138**(6).

[33] Invernizzi, C. M., Iora, P., Preßinger, M., and Manzolini, G., 2016. "HFOs as substitute for R-134a as working fluids in ORC power plants: A thermodynamic assessment and thermal stability analysis". *Appl Therm Eng,* **103**, pp. 790–797.

[34] Zhang, L., Zhuge, W., Zhang, Y., and Chen, T., 2017. "Similarity theory based radial turbine performance and loss mechanism comparison between R245fa and air for heavy-duty diesel engine organic Rankine cycles". *Entropy,* **19**(1).

[35] White, M., and Sayma, A. I., 2015. "System and component modelling and optimisation for an efficient 10 kwe low-temperature organic rankine cycle utilising a radial inflow expander". *P I Mech Eng A-J Pow,* **229**(7), pp. 795–809.

[36] Costall, A. W., Gonzalex-Hernandez, A., Newton, P. J., and Martinez-Botas, R. F., 2015. "Design methodology for radial turbo expanders in mobile organic rankine cycle applications". *Appl Energ,* **157**, pp. 729–743.

[37] Moustapha, H., Zelesky, M. F., Baines, N. C., and Japiske, D., 2003. *Axial and Radial Turbines*. Concepts ETI, Inc.

[38] Dixon, S. L., and Hall, C. A., 2013. *Fluid Mechanics and Thermodynamics of Turbomachinery*, 7th ed. Butterworth-Heinemann.

[39] Cramer, M. S., and Crickenberger, A. B., 1991. "Prandtl-Meyer function for dense gases". *AIAA Journal,* **30**(2), pp. 561–564.

[40] Lemmon, E. W., Huber, M. L., and McLinden, M. O., 2013. NIST standard reference database 23: Reference fluid thermodynamic and transport properties-REFPROP.

[41] White, M., Sayma, A. I., and Markides, C. N., 2017. "Supersonic flow of non-ideal fluids in nozzles : An application of similitude theory and lessons for ORC turbine design and flexible use considering system performance". *J Phys Conf Ser,* **821**.

[42] Rinaldi, E., Pecnik, R., and Colonna, P., 2015. "Unsteady RANS simulation of the off-design operation of a high expansion ratio ORC turbine". In 3rd International Seminar on ORC Power Systems, no. 150.

[43] Maizza, V., and Maizza, A., 1996. "Working fluids in non-steady flows for waste energy recovery systems". *Appl Therm Eng,* **16**(7), pp. 579–590.

[44] White, M., and Sayma, A. I., 2015. "The application of similitude theory for the performance prediction of radial turbines within small-scale low-temperature organic Rankine cycles". *J Eng Gas Turb Power,* **137**(12).

Appendix A: Supersonic stator design

The geometry of the supersonic stator is defined in Fig. 14. The throat width o_{th} is obtained from:

$$o_{\text{th}} = \frac{\dot{m}}{\rho^* a^* b_4 Z_{\text{n}}}, \tag{9}$$

where b_4 is rotor inlet blade height, Z_{n} is the number of stator blades, and ρ^* and a^* are the static choked throat conditions, calculated by assuming an isentropic expansion from T_{01} and P_{01}. The throat Reynolds number is given by:

$$Re_{\text{d}} = \frac{\rho^* a^* D_{\text{h}}}{\mu}, \tag{10}$$

where μ is the viscosity and D_{h} is the hydraulic diameter.

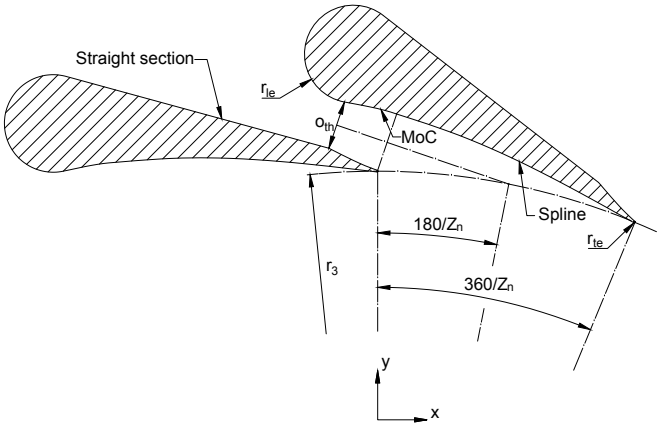

Fig. 14. Geometrical desciption of the supersonic turbine

The geometrical parameters for the two stators are summarised in Tab. 4. The leading-edge radii are set to $r_{\text{le}} = o_{\text{th}}$ and $r_{\text{le}} = 1.5 o_{\text{th}}$ for the R245fa and Toluene stators respectively. The stator is constructed by creating a construction circle at the stator inlet radius. The end point of the bottom half of the diverging nozzle obtained using the MoC model is positioned on this construction circle at the point $(0, r_3)$, and rotated such that the nozzle centreline intersects the construction circle at $\theta = 180/Z_{\text{n}}$. The leading and trailing edges are constructed, and are connected by a straight line to create the subsonic section. The diverging supersonic section is then connected to the trailing edge using a spline.

Table 4. Stator design parameters

	Z_{n}	o_{th}	Re_{d}	r_3	r_{te}	r_{le}
	-	mm	-	mm	mm	mm
R245fa	16	2.97	2.52×10^6	41	0.05	2.97
Toluene	16	1.89	1.09×10^6	41	0.05	2.84